Jurnal Elektronika dan Telekomunikasi (JET), Vol. 25, No. 1, August 2025, pp. 64-70
Accredited by RISTEKDIKTI, Decree No: **158/E/KPT/2021**
doi: 10.55981/jet.723

Implementation of LIDAR for Navigation, Geometric Shape Mapping, and Center of Mass

Mikail Vadim Sena, Faisal Wahab*, Bagus Made Arthaya

Department of Electrical Engineering
Parahyangan Catholic University
Jl. Ciumbuleuit No. 94
Bandung, Indonesia

Abstract

This study examines the ability of Light Detection and Ranging (LIDAR) to enhance autonomous vehicle navigation through laser-based distance measurement. LIDAR technology, which has become increasingly vital in robotics and autonomous vehicles, enables the identification and mapping of objects in real time with high accuracy. The integration of LIDAR with the Robot Operating System (ROS) further enhances the system's capabilities by providing a robust framework for sensor data processing and control algorithms in an autonomous system. In this research, LIDAR is applied to indoor navigation, focusing on mapping objects in the shapes of rectangles, triangles, and circles. The data obtained from LIDAR are used by a condition-based (if-else) navigation system on a mobile robot to determine the dimensions of objects and the location of their center points. The results show that LIDAR can provide effective feedback in navigation systems, with object mapping consistent with preconfigured maps. The recorded mapping error rate is 1.93%, demonstrating that this technology is reliable for autonomous navigation applications.

Keywords: LIDAR; Robot Operating System (ROS); Navigation; Center of mass.

I. INTRODUCTION

Light Detection and Ranging (LIDAR) is a remote sensing method that utilizes laser beams to determine the distance between a sensor and nearby objects. It operates by sending laser pulses toward an object and measuring the time it takes for the pulses to return after bouncing off the object. This time measurement allows a precise calculation of the distance [1]. Because it provides highly accurate environmental data [2] , this study demonstrates that LIDAR, with an accuracy of 92.55%-93.03%, is slightly more accurate than ultrasonic sensors, which achieve 92.20%-92.88%, in measuring the area of complex structures using noncontact methods [3].

To operate the LIDAR sensor, the Robot Operating System (ROS) is used to program the device. ROS is a flexible framework designed to program and control robotic systems [4]. It offers tools, libraries, and guidelines that simplify the development of reliable robot behavior across various platforms. ROS enables hardware abstraction, device control, integration of common functionalities, message passing between processes, and package management. By enabling modular development, ROS allows different software components to communicate seamlessly. In a navigation system, ROS can manage sensor data, control movement, and facilitate real-time decision-making.

LIDAR is widely used in applications such as topographic mapping [5], 2D modeling, and autonomous navigation and robotics [6], as well as mapping tasks that require the identification of the geometric shape of the surrounding objects [7]. LIDAR is crucial for navigation, as it provides highly accurate and detailed environmental maps, allowing autonomous vehicles to detect and avoid obstacles while understanding the contour of the road [8]. Its use is expected to improve transportation safety and efficiency due to its real-time accuracy [9]. In various applications, accurately determining the shape and size of objects is essential for navigation systems to reliably detect and avoid obstacles [10]. Understanding an object's geometry is critical for safe and effective environmental interaction, as well as for creating precise 2D models used in analyzing and mapping complex structures.

The centroid, or center of mass, represents the average position of all points within a geometric shape and is integral to structural analysis, dynamics, and numerous engineering applications [11]. In physics and robotics, the centroid simplifies calculations related to dynamics and stability by providing an average reference point [12]. This point is key in advanced data processing tasks such as object tracking and pattern recognition algorithms. In robotic navigation, knowing the location of the centroid supports optimal route planning, helping to determine whether to approach or avoid obstacles [13]. Furthermore, the identification of the centroid helps to analyze shape and size, which allows for more efficient control strategies to maintain balance and optimize movement [14].

The main contribution of this paper is the implementation of LIDAR for navigation, geometric shape mapping, and the estimation of the center of mass

* Corresponding Author.
Email: faisal.wahab@unpar.ac.id
Received: March 18, 2025 ; Revised: April 25, 2025
Accepted: June 21, 2025 ; Published: August 31, 2025

of detected objects. Detected objects are limited to three basic shapes: rectangles, triangles, and circles.

The structure of the paper is as follows. Section I provides an introduction. Section II explains the proposed methodology for conducting this research. Section III presents the experimental results, discusses the system developed, and highlights the novelty of the research findings. Finally, Section IV concludes the article and outlines limitations and directions for further research.

II. METHODS

The methodology of this study is divided into four parts: LIDAR sensor, design of mobile robot platform and electrical system design, navigation system, and geometrical object mapping and center of mass.

A. LIDAR

The Light Detection and Ranging (LIDAR) sensor used in this paper is the Slamtec A1M8, which can only read the environment in 2D Cartesian coordinates [15]. The operation of this LIDAR is illustrated in Figures 1 and 2.

The scanning process results in a set of points which, when visualized, form a contour resembling a wall. The point s serves as a reference in the global frame, while the point l is part of the local frame originating from the LIDAR's origin. Point P represents one of the LIDAR scan results. The angle between the local x-axis, denoted as x_l, and point P is referred to as θ_1, while the angle between x_l and x_s is called θ_2.

B. Mobile Robot Prototype

The design of a prototype mobile robot equipped with LIDAR for room mapping applications will be explained in this section. An overview of the design for the mobile robot prototype is shown in Figure 3. The robot type employed is a Differential Drive Wheeled Mobile Robot (DDWMR) with two motors, each

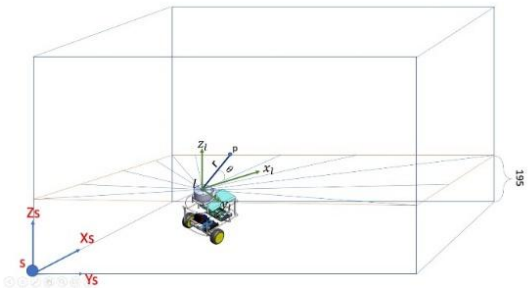

Figure 1. Illustration of LIDAR scanning in a 3D environment.

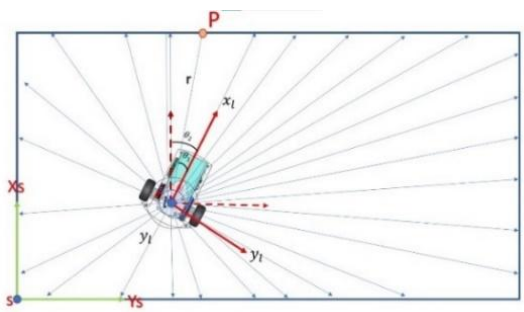

Figure 2. Top view of LIDAR scanning.

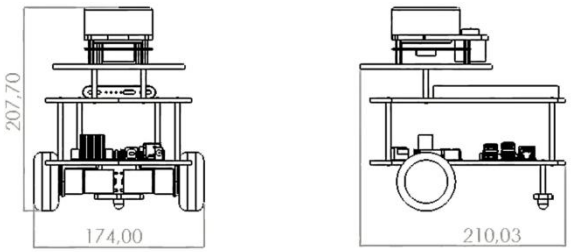

Figure 3. The design of a prototype mobile robot.

controlling a wheel. Movement is achieved by applying Pulse Width Modulation (PWM) to the motors, enabling the wheels to rotate at speeds (ω_r) and (ω_l), which correspond to the right and left wheels, respectively. The robot's direction is determined by the relative speeds of the wheels; to move forward, (V_R) and (V_L) must be the same. In addition to moving forward, the robot can also rotate up to 90 degrees. Rotation is controlled using PWM. To rotate, the speeds of the right and left wheels (ω_r and ω_l) must be opposite.

Following the prototype design, the next step involves the design of the electrical system. The schematic of the electrical design of the mobile robot prototype is shown in Figure 4. In electrical design, an Arduino is used to control both DC motors, while a Raspberry Pi functions as the computer to collect and process LIDAR data. Additionally, the processed data are transmitted to a main computer for visualizing the room scanning results. The scanning results are then sent back from the Raspberry Pi to the Arduino, which subsequently controls the movement of the mobile robot prototype.

C. Navigation System

The navigation system used in this study is based on a simple if-else approach, which effectively guides the system through its environment by making decisions based on predefined conditions. This straightforward method ensures reliable and responsive navigation. The initial definition and configuration are the key to designing a mobile robot's movement algorithm.

To ensure accurate navigation, the starting point must be carefully selected based on movement goals and environmental conditions. The orientation of the robot's movement is illustrated in Figure 5. To run the navigation system, initial information is required, including manually input coordinates and LIDAR scan

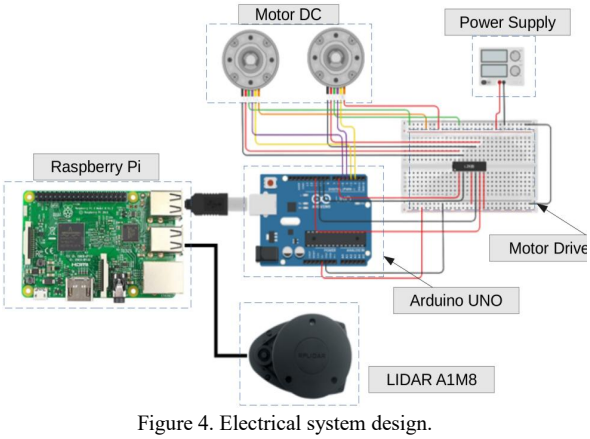

Figure 4. Electrical system design.

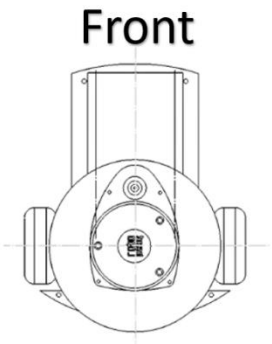

Figure 5. Illustration of robot orientation.

data. Key points, such as the initial position (I_x , I_y) finish position f_x, f_y and initial orientation (north (N), south (S), west (W), and east (E)) in cartesian coordinates (x,y), are shown in Figure 6. The LIDAR nodes are processed to determine the farthest position and the distance between the robot's front and the obstacles ahead (front distance).

Besides the front distance measurement, another reference used is the distance, which represents the robot's distance from the side wall. This measurement is utilized to maintain the robot's distance from the side wall. If the robot gets too close to the wall, it will move away and if it is too far, it will move closer. The purpose of observing the side wall distance is to determine whether LIDAR can be effectively used as feedback during the robot's movement.

Before understanding the robot's movement, it is important to be familiar with certain terms related to the navigation system. These terms are illustrated in Figure 7. From the illustration, Δx represents the distance between the initial position I_x and the point (f_x, I_x). The offset x is the difference between the front distance and Δx . Δy represents the distance between the initial position I_y and the point f_y . The offset y is the difference between the front distance and Δy. From this

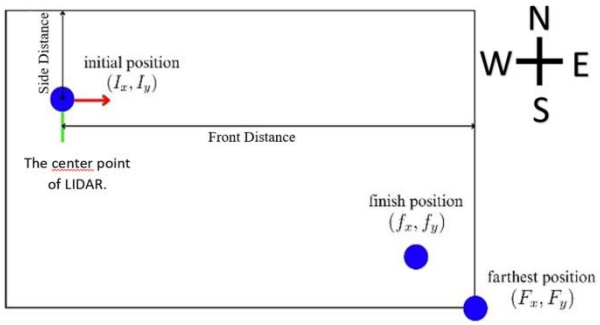

Figure 6. Illustration of the orientation of points in the room.

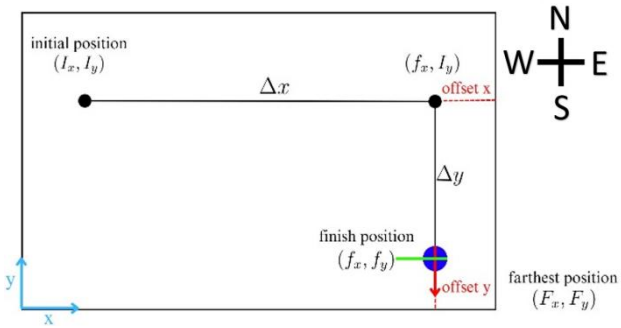

Figure 7. Initial definition of points in the navigation system.

definition, the navigation algorithm flowchart is illustrated in Figure 8.

D. Geometrical Mapping and Center of Mass

The centroid, or center of mass, is the point that represents the average position of the entire mass or area of an object. In a two-dimensional (2D) context, the centroid is often used to determine the geometric midpoint of an irregular shape. The centroid of a 2D area can be defined as the point at which the entire mass or area of the shape is balanced in all directions.

1) Rectangular

For a square and rectangle with length l and width w , and vertices at coordinates (x,y), the centroid coordinates are illustrated in Figure 9. The center of mass of a rectangle in Cartesian coordinates is the midpoint of its coordinates. To find the center of mass of the rectangular, (1) and (2).

$$\bar{x} = \frac{x_2 + x_1}{2} \quad (1)$$

$$\bar{y} = \frac{y_2 + y_1}{2} \quad (2)$$

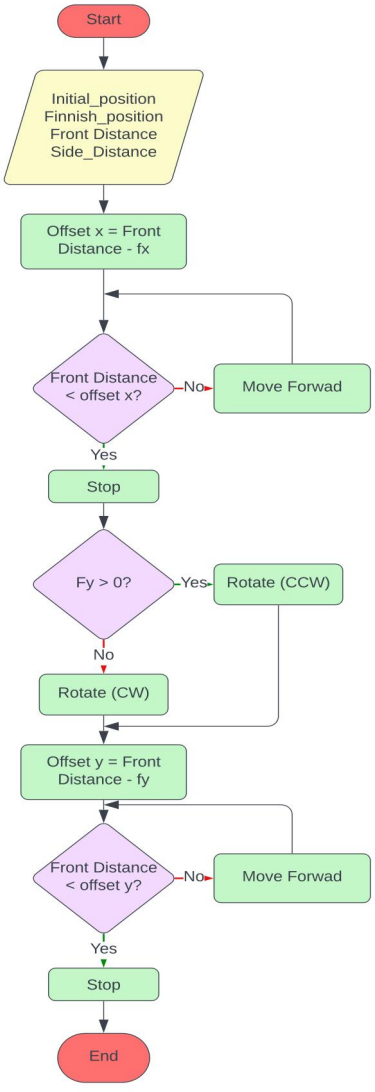

Figure 8. Navigation algorithm flowchart

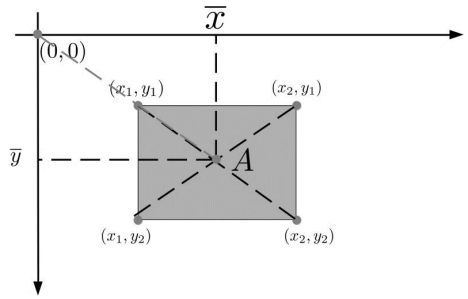

Figure 9. Center of mass of a rectangle.

2) Triangle

The centroid of a triangle is a fundamental concept in geometry, defined as the point where the three medians of the triangle intersect. A median is a line that connects a vertex of the triangle to the midpoint of the opposite side. An illustration of the triangle's centroid can be seen in Figure 10.

Δx represents the distance from the reference point to point A along the x-axis, while Δy denotes the distance from the reference point to the center of mass of A along the y-axis. To determine the center of mass in Figure 10, (3) and (4) are applied. The center of mass of the triangle is denoted as $A = (x, y)$. The value of x is obtained using (3), and the value of y is determine using (4).

$$\bar{x} = x_1 + \Delta x = x_1 + \left(\frac{(x_2 - x_1) + (x_3 - x_1)}{3}\right) \quad (3)$$

$$\bar{y} = y_1 + \Delta y = y_1 + \left(\frac{y_2 - y_1}{3}\right) \quad (4)$$

3) Circular

The centroid of a circle is the point at which the entire mass of the circle can be considered to be concentrated. For a circle, the centroid is always exactly at the center of the circle, which is the center point itself. An illustration of the circle's center is provided in Figure 11.

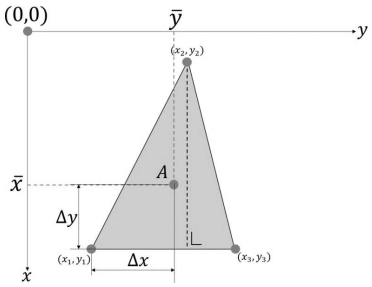

Figure 10. Center of mass of a triangle.

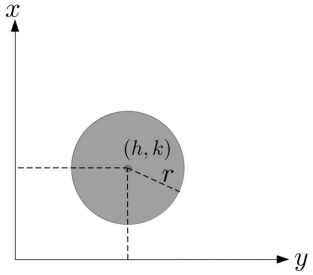

Figure 11. Center of mass of a circle.

The centroid A of a circle centered at (h, k) with radius r is given by (5).

$$(\bar{x}, \bar{y}) = (h, k) \quad (5)$$

The center of mass (centroid) of a circle lies at its geometric center, as a result of the circle's perfect symmetry.

III. Result And Discussion

A. Mobile Robot Platform

Figure 12 shows the real robot used in this experiment. The LIDAR sensor is mounted on the top layer of the robot. The second layer houses the Raspberry Pi and microcontroller, while the third layer accommodates the battery pack and driver motor. The Raspberry Pi is connected to the laptop with a Wi-Fi network.

B. Navigation

Navigation is observed based on front and side distances measurements to determine the optimal movement of the mobile robot. The navigation results can be observed from the front distance data presented in the graph shown in Figure 13.

From time ($t = 0$) to approximately($t \approx 45$), the robot remains stationary at point (0,0). The robot begins to move around ($t \approx 46$), as indicated by a decrease in the front distance value. When the front distance value reaches 0.5, the robot stops, as shown at ($t \approx 70$), where the front distance remains constant. This behavior indicates that the robot can respond to commands based on the front distance readings, allowing it to navigate according to the preconfigured navigation system.

At ($t \approx 79$), the robot rotates 90 degrees, which is reflected in the graph showing a front distance of 1.5 again. Then, at ($t \approx 103$) , the robot resumes

Figure 12. The mobile robot platform.

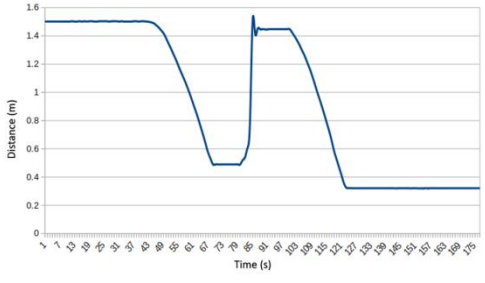

Figure 13. Front distance data.

movement, as indicated by the decreasing distance on the graph. However, in this instance, the robot does not stop as expected. Instead of stopping at the set distance of 0.5, it halts at 0.3. This discrepancy is likely due to a processing error in the navigation system based on LIDAR readings.

For side distance navigation, the LIDAR sensor measures the distance to the wall beside the robot, enabling it to follow the wall's contour and stay on the correct path. Control for side distance navigation uses a simple if-else approach. If the side distance is greater than 0.5, the robot will turn left to reduce the distance. On the contrary, if the side distance is less than 0.5, the robot will turn right to increase the distance. This setup ensures that the robot maintains a consistent distance of 0.5 from the wall. The side distance data are shown in Figure 14.

In Figure 14, several data analyses can be performed. At time $(t = 0)$ to approximately $(t \approx 45)$, the robot remains stationary at point (0,0), with a side distance reading of 0.486. Once the robot starts moving, the system adjusts the distance to approach 0.5. At $(t \approx 79)$, the robot turns 90 degrees, causing a brief spike in the distance reading. After the turn, the robot overshoots 90 degrees, leading to a side distance reading above 0.5. The robot resumes movement at $(t \approx 103)$, and because the side distance is greater than 0.5, the system instructs the robot to turn right, decreasing the distance toward 0.5. At around $(t \approx 117)$, the robot crosses the 0.5 side distance threshold. As the system detects that the distance is now less than 0.5, the robot turns right again. The graph shows that after crossing 0.5, the distance increases as expected. However, the system's delayed response causes the robot to stop at a position different from the intended target.

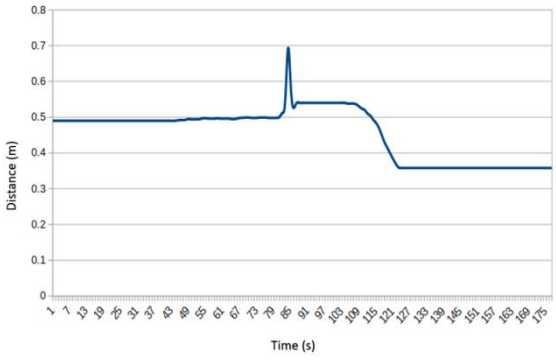

Figure 14. Side distance data.

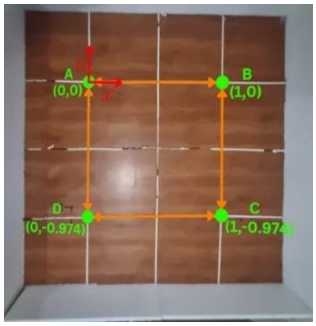

Figure 15. Top view of the LIDAR scan.

C. Geometrical Mapping and Center of Mass

The test area and robot's movement are described before testing, as shown in Figure 15. The testing area measures 2.020 × 1.950 meters and is enclosed by wooden walls with a height of 50 cm. Four checkpoints are defined within the area: A, B, C, and D. For data collection, the robot follows a predefined path, moving sequentially from point A to B, B to C, C to D, and finally returning to point A.

The reference objects used in the experiment are a rectangle, a triangle, and a circle, as shown in Figure 16. Each object is placed randomly on the map, with its position and orientation adjusted to observe changes in the mapping results. After completing the mapping process, the results for each object are obtained and their dimensions and centroids are determined and analyzed.

1) Rectangle

The position and orientation of the rectangle were tested under three different conditions. The rectangle has a length of 0.33 meters and a width of 0.265 meters. The corresponding mapping results are shown in Figure 17. From the three mapping results, it is evident that the LIDAR system can accurately map the rectangular object, even under variations in position and orientation. Using the line equation method, the length and width of the three rectangles were determined, as shown in Table 1.

The data collection process is divided into several steps. The first step is to measure the length and width

Figure 16. Reference objects: rectangle, triangle, and circle.

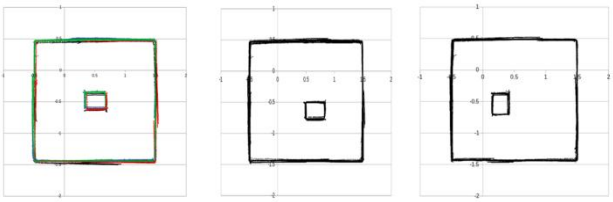

(a) (b) (c)

Figure 17. (a) The rectangle is placed in the center. (b) The position of the rectangle is changed. (c) Both the position and orientation of the rectangle are altered.

TABLE 1
COMPARISON OF RECTANGLE MEASUREMENTS

Real and Measured			
Real(m)	**Placement**	**Measured(m)**	**Error**
Length (0.33)	Position 1	0.3383	2.52%
	Position 2	0.3369	2.1%
	Position 3	0.3292	0.24%
Average			**1.62%**
Width (0.265)	Position 1	0.2575	2.83%
	Position 2	0.2599	1.92%
	Position 3	0.2597	2%
Average			**2.23%**

of the object. In the length measurement process, LIDAR readings are used to obtain the lines on the left and right x-axes. Each axis is processed using linear regression, which is applied to all sides. After obtaining the line equations for the left and right x-axes, the distance calculation is performed. The determination of the line equations and the rectangular points is shown in Figure 18.

Table 1 shows the comparison between the real and measured rectangle dimensions. The actual length of the rectangle is 0.33 meters, while the measured values range from 0.3292 to 0.3383 meters, resulting in errors between 0.24% and 2.52%, with an average error of 1.62%. Similarly, the actual width is 0.265 meters, and the measured values range from 0.2575 to 0.2599 meters, leading to errors between 1.92% and 2.83%, with an average error of 2.23%. The overall average error of 2.23% suggests that the system performs well with minimal deviation from the actual values. To obtain the dimensions, the centroids of the three positions were also determined, as shown in Table 2.

The centroid is determined based on the position and orientation of the rectangle in the test area and is calculated using the linear regression results. From the testing and data analysis, the rectangle's dimensions have an average length of 0.3348 ± 0.0049 m and an average width of 0.259 ± 0.0013 m, with their respective standard deviations.

2) *Triangle*

The next experiment used a triangular geometric object. Unlike the rectangle, the triangle has three sides, with two being sloped. The mapping results using LIDAR are shown in Figures 19 and 20. Using the same steps as for the rectangle, the analysis of the base, height and centroid of the triangle was obtained, as shown in Table 3.

From the testing and data processing of the triangle, the average and standard deviation of the base were 0.2518 ± 0.00567 m, while the height was 0.2779 ± 0.00201 m. These results indicate that the variability in the height of the triangle is greater than that of its base. This difference is likely due to the lower regression accuracy when averaging the line equations on the inclined sides, leading to greater deviations in the measurements.

3) *Circular*

The next experiment involved a circular geometric object. Unlike triangles and rectangles, which have multiple sides and angles, the circle has only one continuous side and no angles. The mapping results are shown in Figures 21 and 22. From the two mapping results, the radius and centroid of the circle were determined, as shown in Table 4. From the measurements, the average radius of the circle was 0.1005 ± 0.000707 m**.** The circle has the smallest standard deviation among the geometric objects. This is due to the lack of sides of the circle, referring to the determination of the radius dependent on the centroid. Additionally, precise testing ensures that the distance

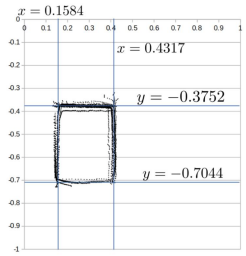

(a)

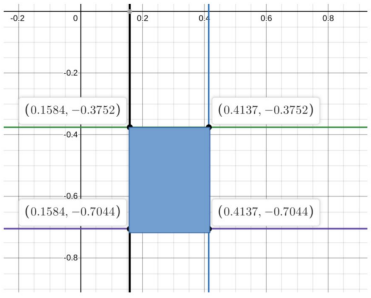

(b)

Figure 18. (a) Determination of the line equation. (b) Determination of the rectangle points.

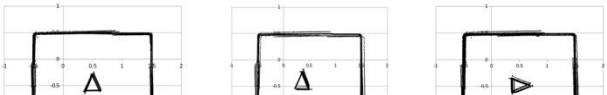

(a) (b) (c)

Figure 19. (a) The triangle is placed in the center. (b) The position of the triangle is changed. (c) Both the position and orientation of the triangle are altered.

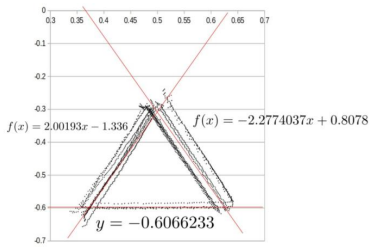

(a)

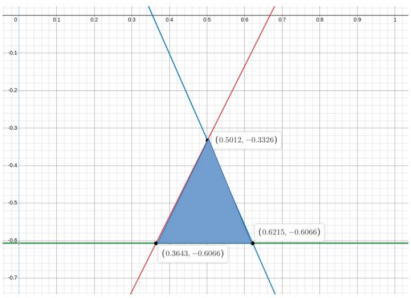

(b)

Figure 20. (a) Determination of the line equation. (b) Determination of the rectangle points.

TABLE 2
CENTROID ANALYSIS RESULTS FOR THE RECTANGLE

Placement	Centroid(x,y)
Position 1	(0.5195,-0.4868)
Position 2	(0.6581,-0.6448)
Position 3	(0.3653,-0.5398)

TABLE 3
RESULT OF THE BASE, HEIGHT, AND CENTROID OF THE TRIANGLE

Placement	Base(m)	Height(m)	Centroid
Position 1	0.2572	0.2742	(0.499,-0.5153)
Position 2	0.2523	0.2599	(0.3632,-0.4425)
Position 3	0.2459	0.2996	(0.4714,-0.4812)

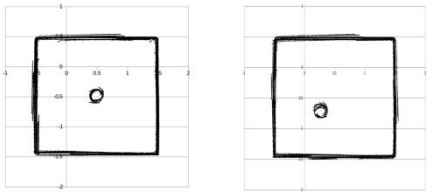

(a) (b)

Figure 21. (a) The circular is placed in the center. (b) The position of the circular is changed.

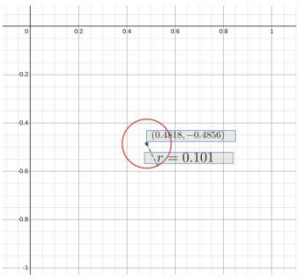

Figure 22. Determination of the circular points.

TABLE 4
RESULT OF THE RADIUS AND CENTROID OF THE CIRCLE

Placement	Radius(m)	Centroid
Position 1	0.101	(0.4818,-0.4859)
Position 2	0.1	(0.2676,-0.7005)

from the centroid to each point in the LIDAR data is close to the average radius value.

IV. CONCLUSION

From the navigation experiments conducted, it can be concluded that the LIDAR sensor can be used as a feedback in the navigation of mobile robots. The LIDAR sensor effectively detects positional changes through rapid distance measurements. Based on the geometric object mapping results, it can be concluded that the shape, position, and orientation of the mapped objects remain consistent with the initial setup. This indicates that the LIDAR system used maintains accuracy and precision in visualizing objects. Additionally, the average error rate obtained from the geometric object mapping method is 1.93%. With its high accuracy, LIDAR technology is highly suitable for various applications. For further development, the system should be tested in dynamic environments to evaluate its performance in responding to rapid changes and moving objects. Furthermore, a robot control system based on LIDAR feedback can be developed, such as for autonomous navigation and real-time obstacle avoidance.

DECLARATIONS

Conflict of Interest

The authors have declared that there are no competing interests.

CRediT Authorship Contribution

Mikail Vadim Sena: Software, Investigation, Resources, Writing-Original draft preparation, Data Curation, Visualization; Faisal Wahab: Supervision, Conceptualization, Methodology, Writing-Reviewing and Editing; Bagus Made Arthaya: Formal analysis, Supervision, Investigation and Validation.

Funding

The author(s) received no financial support for the research, authorship, and/or publication of this article.

Acknowledgment

The authors would like to thank the Electrical Engineering Department and Parahyangan Catholic University for providing the academic and research environment that supported this study.

REFERENCES

[1] D. F. Pozo, L. Morales, D. Pozo, K. Jaramillo, D. Ponce, and A. Torres, “3D reconstruction technologies for using in dangerous environments with lack of light: a comparative analysis," RISTI - Rev. Ibér. Sist. Tecnol. Inf., Aug. 2019.

[2] Q. Zou, Q. Sun, L. Chen, B. Nie and Q. Li, "A Comparative Analysis of LiDAR SLAM-Based Indoor Navigation for Autonomous Vehicles," in IEEE Trans. Intell. Transp. Syst., vol. 23, no. 7, pp. 6907-6921, July 2022, doi: 10.1109/TITS.2021.3063477

[3] C. K J and A. V M, "Investigation on Accuracy of Ultrasonic and LiDAR for Complex Structure Area Measurement," in Proc. Int. Conf. Trends Elect. Inf. (ICOEI), Tirunelveli, India, 2022, pp. 134-139, doi: 10.1109/ICOEI53556.2022.9777233.

[4] S. Macenski, T. Foote, B. Gerkey, C. Lalancette, and W. Woodall, "Robot operating system 2: design, architecture, and uses in the wild," Sci. Robot., vol. 7, no. 66, May 2022, doi: 10.1126/scirobotics.abm6074.

[5] C. Wei and Z. Jian, "Application of intelligent UAV onboard LiDAR measurement technology in topographic mapping," in Proc. IEEE Int. Conf. Emerg. Sci. Inf. Technol. (ICESIT), 2021, pp. 942–945, doi: 10.1109/ICESIT53460.2021.9696811.

[6] M. Royhan Iqbal, A. Husein Alasiry, H. Oktavianto, A. Darmawan, A. Teguh Budi Antok and I. Kresno Wibowo, "Corner Detection with 2-D RPLIDAR to Detect Furniture on TCIFFRC Tracks," in Proc. Int. Elect. Symp (IES), Surabaya, Indonesia, 2020, pp. 297-301, doi: 10.1109/IES50839.2020.9231648.

[7] Y. Qi *et al.*, “Geometric information constraint 3d object detection from lidar point cloud for autonomous vehicles under adverse weather,” *Transp Res Part C Emerg Technol*, vol. 161, p. 104555, 2024, doi: https://doi.org/10.1016/j.trc.2024.104555.

[8] P. Leong and N. Ahmad, “LiDAR-based obstacle avoidance with autonomous vehicles: a comprehensive review,” *IEEE Access*, vol. PP, p. 1, Jan. 2024, doi: 10.1109/ACCESS.2024.3493238.

[9] A. Ansariyar and M. Jeihani, “Investigating lidar sensor accuracy for v2v and v2p conflict detection at signalized intersections,” *Future Transportation*, vol. 4, no. 3, pp. 834–855, 2024, doi: 10.3390/futuretransp4030040.

[10] K. Suzuki, R. Shinkuma, N. Nakamura, and G. Trovato, "Spatial model for capturing size and shape of object from point cloud data for robot vision system with lidar sensors," in Proc. IEEE Consum. Commun. Netw. Conf. (CCNC), 2023, pp. 493–496, doi: 10.1109/CCNC51644.2023.10060006.

[11] A. Gahramanova, "Locating centers of mass with image processing," Undergrad. J. Math. Model.: One + Two, vol. 10, Mar. 2019, doi: 10.5038/2326-3652.10.1.4906.

[12] D. Orin, A. Goswami, and S.-H. Lee, “Centroidal dynamics of a humanoid robot,” *Auton Robots*, vol. 35, Mar. 2013, doi: 10.1007/s10514-013-9341-4.

[13] T. Yong, G. He, W. Y. Fang, and L. Jiang Bo, "A movement planning and control method of special robot over obstacle based on centroid monitoring," in Proc. IEEE Int. Conf. Robot. Biomimetics (ROBIO), 2021, pp. 1902–1908, doi: 10.1109/ROBIO54168.2021.9739556.

[14] M. Aranda, J. A. Corrales, and Y. Mezouar, "Deformation-based shape control with a multirobot system," in Proc. IEEE Int. Conf. Robot. Autom. (ICRA), 2019, pp. 2174–2180, doi: 10.1109/ICRA.2019.8793811

[15] S. Bi, C. Yuan, C. Liu, J. Cheng, W. Wang, and Y. Cai, “A survey of low-cost 3d laser scanning technology,” *Applied Sciences (Switzerland)*, vol. 11, no. 9. MDPI AG, 2021. doi: 10.3390/app11093938.